Clarity through the Neutrino Fog: Constraining New Forces in Dark Matter Detectors

Pablo Blanco-Mas,[1, *] Pilar Coloma,[1, †] Gonzalo Herrera,[2, ‡] Patrick Huber,[2, §]
Joachim Kopp,[3, 4, ¶] Ian M. Shoemaker,[2, **] and Zahra Tabrizi[3, 5, ††]

[1]*Instituto de Física Teórica UAM-CSIC, Calle Nicolás Cabrera 13–15,
Universidad Autónoma de Madrid, 28049 Madrid, Spain*
[2]*Center for Neutrino Physics, Department of Physics, Virginia Tech, Blacksburg, VA 24061, USA*
[3]*Theoretical Physics Department, CERN, 1 Esplanade des Particules, CH-1211 Geneva 23, Switzerland*
[4]*PRISMA+ Cluster of Excellence & Mainz Institute for Theoretical Physics, 55128 Mainz, Germany*
[5]*PITT PACC, Department of Physics and Astronomy,
University of Pittsburgh, 3941 O'Hara St., Pittsburgh, PA 15260, USA*

The PANDAX-4T and XENONnT experiments present indications of Coherent Elastic Neutrino Nucleus Scattering (CEνNS) from ^{8}B solar neutrinos at 2.6σ and 2.7σ, respectively. This constitutes the first observation of the neutrino "floor" or "fog", an irreducible background that future dark matter searches in terrestrial detectors will have to contend with. Here, we first discuss the contributions from neutrino–electron scattering and from the Migdal effect in the region of interest of these experiments, and we argue that they are non-negligible. Second, we make use of the recent PANDAX-4T and XENONnT data to derive novel constraints on light scalar and vector mediators coupling to neutrinos and quarks. We demonstrate that these experiments already provide world-leading laboratory constraints on new light mediators in some regions of parameter space.

1. INTRODUCTION

Recently, the PANDAX-4T collaboration has reported the first measurement of the neutrino fog from coherent elastic neutrino–nucleus scattering (CEνNS) of solar ^{8}B neutrinos [1] at 2.6σ. This was soon followed by an announcement of the XENONnT collaboration, which reported the measurement of CEνNS at 2.7σ [2]. Both experiments observed the signal using the combined ionization and scintillation (S1+S2) signal. PANDAX-4T also reported a signal in the S2 (ionization) channel separately. Interestingly, while for the combined analysis both experiments report background expectations consistent with the observed event rates, this is not the case for the S2-only analysis at PANDAX-4T, where an excess with respect the background expectation of a few tens of events is observed. Using a Poissonian likelihood of the number of signal and background events, the excess has a low significance of 1.3σ for science Run0, but a somewhat larger significance of 3.6σ for Run1.

The fact that dark matter direct detection experiments could provide sensitivity to Beyond the Standard Model (BSM) interactions of solar neutrinos was pointed out about a decade ago, and a series of works have followed through the years discussing various BSM scenarios, different interaction channels of neutrinos with the detector, and the complementarity of different experiments and detector technologies [3–13]. In light of the recent datasets from XENONnT and PANDAX-4T, some works have constrained non-standard interactions of neutrinos with quarks [14, 15],[1] corresponding to new mediators with masses much larger than the momentum transfer of the scattering process, of order $q = \sqrt{2m_A E_{\rm nr}} \lesssim 10\,\text{MeV}$ at direct detection experiments. (Here, m_A is the mass of the target nucleis and $E_{\rm nr}$ is the nuclear recoil energy.) Here we will study instead the current sensitivity of PANDAX-4T and XENONnT to *light mediators* via CEνNS of ^{8}B solar neutrinos at the detector, making use of the combined (S1+S2) signal as well as the PANDAX-4T S2-only dataset. We will consider in particular light vector mediators with universal couplings to all quarks and neutrinos, as well as light scalar mediators with either universal couplings, or couplings proportional to the quark masses (as in the case of coupling through mixing with the SM Higgs field). We will demonstrate that in some regions of parameter space, these experiments provide complementary and even stronger constraints to other experiments sensitive to CEνNS such as COHERENT [17], whose sensitivity to light new mediators has been widely studied in a series of works, *e.g* [18–24].[2]

The paper is organized as follows: In Section 2, we discuss the different scattering processes that neutrinos can undergo in a liquid xenon detector, showing that CEνNS yields the dominant event rate in the Region of Interest (ROI) of the PANDAX-4T and XENONnT experiments, although the Migdal effect and elastic neutrino–electron

---

* pablo.blanco@ift.csic.es
† pilar.coloma@ift.csic.es
‡ gonzaloherrera@vt.edu
§ pahuber@vt.edu
¶ jkopp@cern.ch
** shoemaker@vt.edu
†† z_tabrizi@pitt.edu

---

[1] The XENONnT and PANDAX-4T datasets have also been used to constrain the uncertainty in the weak mixing angle at low momentum transfer in Ref. [16].

[2] We will restrict ourselves to derive upper limits on the coupling of the mediator to quarks and neutrinos, even though the excess events in the S2-channel of PANDAX-4T could in principle be interpreted as a hint for a positive signal.

scattering can yield sizable contributions (Section 2.1. We then discuss how extensions of the SM with light scalar or vector mediators can modify these rates (Sections 2.2 and 2.4. We present and discuss our results in Section 3, showing in particular parameter space exclusions for the different BSM scenarios. We conclude in Section 4.

2. NEUTRINO INTERACTIONS IN LIQUID XENON DETECTORS

Solar neutrinos reaching direct detection experiments on Earth can leave ionization signatures in liquid noble gas detector through three distinct processes: CEνNS [25, 26], the Migdal effect following CEνNS [9, 27], and elastic neutrino–electron scattering [28–30]. In this section, we will discuss the event rates for all these processes. We will argue that in the Regions of Interest (ROIs) of the recent PANDAX-4T and XENONnT analyses, CEνNS indeed is the dominant process, but the Migdal effect and neutrino–electron scattering can also yield sizable contributions.
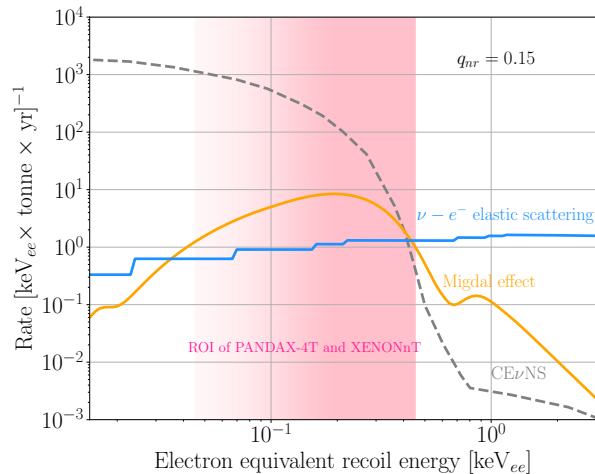

FIG. 1. Comparison of ionization rates induced by ^{8}B solar neutrinos in a liquid xenon detector via different SM processes: CEνNS (grey), the Migdal effect (orange), and elastic neutrino–electron scattering (blue). For CEνNS, a constant quenching factor $q_{nr} = 0.15$ is assumed to translate nuclear recoil energies into electron-equivalent recoil energies. For comparison, we show in shaded pink the approximate ROI of the recent PANDAX-4T and XENONnT analyses of solar neutrinos [1, 2]. The color gradient highlights the fact that the efficiency function is not constant at the ROI of these experiments, but rather increases with energy. The signal induced by CEνNS clearly dominates in the ROI of these experiments, but the Migdal and neutrino–electron scattering contributions are non-negligible. Note that here we have not applied any efficiency factors to the expected ionization rates.

2.1. Standard Model

2.1.1. CEνNS

In the SM, the differential cross section for CEνNS, as a function of the nuclear recoil energy $E_{\rm nr}$, reads [31]

$$\frac{d\sigma_{\nu N - \nu N}}{dE_{\rm nr}} = \frac{G_F^2 m_A}{\pi} Q_V^2 \left(1 - \frac{m_A E_{\rm nr}}{2E_\nu^2}\right), \qquad (1)$$

where m_A is the mass of the target nucleus and Q_V is its vector charge,

$$Q_V = (g_{pV} Z + g_{nV} N) F_A(E_{\rm nr}), \qquad (2)$$

with F_N denoting the nuclear form factor. Here we adopt the prescription from [4, 32]. Here, Z and N stand for the numbers of protons and neutrons in the nucleus, respectively, and the SM neutral current vector couplings are $g_{pV} = \frac{1}{2} - 2\sin^2\theta_W$ and $g_{nV} = -\frac{1}{2}$, with θ_W the Weinberg angle. The differential scattering rate is obtained from the convolution of the differential cross section with the solar neutrino flux

$$\frac{dR^{\rm CE\nu NS}}{dE_{\rm nr}} = \epsilon(E_{\rm nr}) N_T \int_{E_\nu^{\rm min}}^{E_\nu^{\rm max}} \frac{d\Phi}{dE_\nu} \frac{d\sigma_{\nu N \to \nu N}}{dE_{\rm nr}} dE_\nu \quad (3)$$

where N_T the number of xenon (Xe) target nuclei in the detector, $\epsilon(E_{\rm nr})$ is the detection efficiency of the experiment, and $\frac{d\Phi}{dE_\nu}$ is the differential neutrino flux as a function of the neutrino energy.

In the limit where the nuclear mass largely exceeds the nuclear recoil energy, $m_A \gg E_{\rm nr}$ (applicable here since we only consider recoil energies as large as $3\,{\rm keV}$), the minimum neutrino energy needed to induce a recoil $E_{\rm nr}$ is given by

$$E_\nu^{\rm min} = \sqrt{m_A E_{\rm nr}/2}, \qquad (4)$$

while $E_\nu^{\rm max}$ is the kinetic endpoint for the ^{8}B spectrum. We take the expected ^{8}B flux from [33–35], consistent with measurements from Borexino [36]. For CEνNS, we have checked that in nuclear recoil energy windows of the PANDAX-4T and XENONnT analyses, the contribution from ^{8}B largely exceeds the contribution from the other solar neutrino fluxes. For neutrino–electron scattering, on the other hand, it is the contribution from pp solar neutrinos [35] that dominates.

2.1.2. Migdal Effect

Part of the ionization (S2) signal in a nuclear recoil event is due to the Migdal effect [37], which describes the response of atomic electrons to the nucleus receiving a kick. The corresponding differential cross section is obtained by multiplying the cross section for neutrino–nucleus scattering with an ionization form factor $|Z_{\rm ion}(E_{\rm er})|^2$, which accounts for the ionization probabilities of the xenon atom orbitals, see Ref. [9]. This form factor depends on the electron recoiling energy $E_{\rm er}$

and is given by

$$|Z_{\text{ion}}(E_{\text{er}})|^2 = \frac{1}{2\pi} \sum_{n,l} p_{nl \to E_{\text{er}}}, \tag{5}$$

where the differential transition probability of an electron in the orbital (n, l) to an unbound state with recoil energy E_{er} is denoted by $p_{nl \to E_{\text{er}}}$. We take the ionization probabilities for Xe from Ref. [38], taking into account the orbitals $5p$, $5s$, $4d$, $4p$, $4s$, $3d$, $3p$, and $3s$. The electron equivalent energy spectrum due to the Migdal effect can then be calculated as

$$\frac{dR^{\text{mig}}}{dE_{\text{det}}} = N_T \int dE_{\text{nr}}\, dE_{\text{er}}\, \delta(E_{\text{det}} - q_{\text{nr}} E_{\text{nr}} - E_{\text{er}} + |E^{nl}|)$$
$$\times \epsilon(E_{\text{nr}}) \int_{E_\nu^{\text{min}}}^{E_\nu^{\text{max}}} dE_\nu\, \frac{d\Phi}{dE_\nu} \frac{d\sigma_{\nu N \to \nu N}}{dE_{\text{nr}}} \times |Z_{\text{ion}}(E_{\text{er}})|^2. \tag{6}$$

where E_{det} is the measured electron equivalent energy in a liquid Xe detector. Here, E_{nr} is the nuclear recoil energy, E_{er} is the recoil energy of the ionized electron, E^{nl} is its orbital binding energy before the interaction, and q_{nr} is the quenching factor that relates nuclear recoil energies to electron–equivalent recoil energies. The integration over nuclear recoils lies in the kinematical range

$$\frac{\left(E_{\text{er}} + |E^{nl}|\right)^2}{2m_A} < E_{\text{nr}} < \frac{\left(2E_\nu - \left(E_{\text{er}} + |E^{nl}|\right)\right)^2}{2\left(m_A + 2E_\nu\right)}. \tag{7}$$

As previously discussed, we take $q_{\text{nr}} = 0.15$ [38]. It should be noted that the quenching factor (or scintillation efficiency) in liquid xenon is uncertain for low-energy nuclear recoils, with measurements ranging from $q_{\text{nr}} = 0.05$ to 0.2, see, *e.g.*, [39–42].

2.1.3. *Neutrino–Electron Scattering*

Neutrinos can also scatter off electrons in the atom elastically. In this case, the cross section can be calculated using the free-electron approximation, which accounts for the binding energy of electrons in the atom via a Heaviside function [43–45].[3] In this approximation, the differential scattering cross section for neutrinos of flavor $\alpha = e, \mu, \tau$ on electrons is

$$\frac{d\sigma_\alpha}{dE_{\text{er}}} = \sum_{n,l} \theta(E_{\text{er}} - |E^{nl}|) \frac{d\sigma_\alpha^0}{dE_{\text{er}}}, \tag{8}$$

with the cross section for neutrino scattering on free electrons ($\nu_\alpha + e \to \nu_\alpha + e$) given by [47]

$$\frac{d\sigma_\alpha^0}{dE_{er}} = \frac{2G_F^2 m_e}{\pi} \left[g_{L\alpha}^2 + g_{R\alpha}^2 \left(1 - \frac{E_{\text{er}}}{E_\nu}\right)^2 - g_{L\alpha} g_{R\alpha} \frac{m_e E_{\text{er}}}{E_\nu^2} \right]. \tag{9}$$

---

[3] A calculation including the atomic wave functions of xenon yields an event rate smaller by 20–25% [46].

Here, $g_{Le} = (g_V + g_A)/2 + 1$, $g_{L\mu} = g_{L\tau} = (g_V + g_A)/2$, and $g_{R\alpha} = (g_V - g_A)/2$, with $g_V = -1/2 + 2\sin^2\theta_W$ and $g_A = -1/2$. The differential recoil rate is then

$$\frac{dR}{dE_{\text{er}}} = \epsilon N_T \sum_\alpha \int_{E_\nu^{\text{min}}}^{E_\nu^{\text{max}}} dE_\nu\, \frac{d\phi^\alpha}{dE_\nu} \frac{d\sigma_\alpha}{dE_{\text{er}}} \tag{10}$$

where the minimum neutrino energy required to induce a given recoil energy is now given by

$$E_\nu^{\text{min}} = \frac{E_{\text{er}} + \sqrt{2m_e E_{\text{er}} + E_{\text{er}}^2}}{2}. \tag{11}$$

(Note that, in contrast to Eq. (4), we have here kept terms suppressed by E_{er}/m_e, given that this ratio, while still small, is larger than the corresponding one for nuclear recoils, E_{nr}/m_A.)

The ionization rates due to CEνNS, the Migdal effect, and neutrino–electron scattering are shown in Fig. 1. We see that CEνNS is the dominant contribution in the low recoil energy ROI from Refs. [1, 2], while the contributions from the Migdal effect and from elastic neutrino–electron scattering are smaller, but not entirely negligible. In particular, they are comparable to CEνNS at the upper end of the ROI, and at higher energies they dominate. This raises the question to what extent the Migdal effect and neutrino–electron scattering may affect the PANDAX-4T and XENONnT results, which do not explicitly include these contributions in their signal predictions [1, 2]. For the combined S1+S2 analyses, neglecting neutrino–electron scattering is certainly justified as these events yield a larger S2/S1 ratio than CEνNS, allowing for efficient discrimination. This is also true for the Migdal effect involving K-shell and L-shell electrons [48, 49]. M- and N-shell electrons, however, which are ejected from their host atoms more frequently thank inner-shell electrons due to their lower binding energies, lead to signals very similar to the main nuclear recoil signal. They may therefore not be negligible.

In an analysis using only the S2 signal, both neutrino–electron scattering and the Migdal effect contribute. Still, for the PANDAX-4T S2-only analysis discussed here, the corresponding contributions are still small. Using the efficiency function from Ref. [1], the total number of neutrino–electron scattering events in the ROI is predicted to be of $O(0.1)$, while the Migdal effect contributes $O(1)$ event. This should be compared to the total number of 43 expected solar neutrino CEνNS events in the ROI.

The relative importance of the Migdal effect and neutrino–electron scattering compared to CEνNS depends crucially on the quenching factor (or scintillation efficiency) of liquid xenon at such small energies, which is uncertain. The qualitative discussion presented previously should therefore be taken with a grain of salt. The value that we use, $q_{\text{nr}} = 0.15$, is in overall good agreement with the majority of measurements of the quenching factor [39–42] and with the Lindhard model prediction [50].

In our search for physics beyond the SM, we will only include CEνNS, neglecting the Migdal effect and

neutrino–electron scattering. This approach can be regarded conservative since including additional contributions to the SM background would reduce the room there is for new physics.[4]

2.2. A New Scalar Mediator

In extensions of the SM, neutrinos may experience new interactions with nuclei. We will in the following consider the possibility that neutrinos couple to a new scalar mediator ϕ which also couples to quarks. Below, we will then extend the discussion also to new vector mediators. For the scalar case, the relevant terms in the Lagrangian read

$$\mathcal{L} \supset \phi\left(g_\nu \bar{\nu}_R \nu_L + g_q \bar{q}q + \text{h.c.}\right) - \frac{1}{2}m_\phi^2\phi^2\,, \qquad (12)$$

where m_ϕ is the mass of the scalar and g_q, g_ν are dimensionless coupling constants. We will consider both the case that g_q is the same for all quark flavors and the case that g_q scales with the quark masses. The latter scenario is motivated by models in which the new scalar couples to quarks through mixing with the SM Higgs boson. It corresponds to the replacement

$$g_q \to \frac{g_q m_q}{v_H} \qquad (13)$$

in Eq. (12), where $v_H = 246\,\text{GeV}$ is the SM Higgs vev. The contribution due to a new scalar interaction would not interfere with the SM one because of the different Lorentz structures. The scalar-induced CEνNS cross section reads [5, 51]

$$\left(\frac{d\sigma_{\nu N - \nu N}}{dE_{\text{nr}}}\right)_\phi = \frac{g_\nu^2 \mathcal{Q}_\phi^2 m_A^2}{4\pi}\frac{E_{\text{nr}}}{E_\nu^2(2m_A E_{\text{nr}} + m_\phi^2)^2}, \quad (14)$$

where the scalar "charge" is defined as [52]

$$\mathcal{Q}_\phi = \left[Z\sum_{q=u,d,s} g_q \frac{m_p}{m_q} f_{T_q}^p + N\sum_{q=u,d,s} g_q \frac{m_n}{m_q} f_{T_q}^n\right] F_N(E_{\text{nr}}). \qquad (15)$$

We take values of the hadronic form factors $f_{T_q}^p$ and $f_{T_q}^n$ from Ref. [53]. We have compared our definition of the scalar charge for Xenon with that from [54], which is computed using a nuclear shell model, finding that at the low recoil energies of interest to us, the two expressions differ by at most 10%.

The scalar-mediated scattering rate is then obtained in full analogy to Eq. (10), but with the SM cross-section replaced by Eq. (14).

---

[4] In general, physics beyond the SM will also contribute to the Migdal effect and to neutrino–electron scattering. However, as long as the new physics-induced event rates are much smaller than the SM ones, and the Migdal/CEνNS and ν–e scattering/CEνNS ratios are similar for new physics processes and SM processes, it remains true that neglecting the Migdal effect and neutrino–electron scattering is conservative.
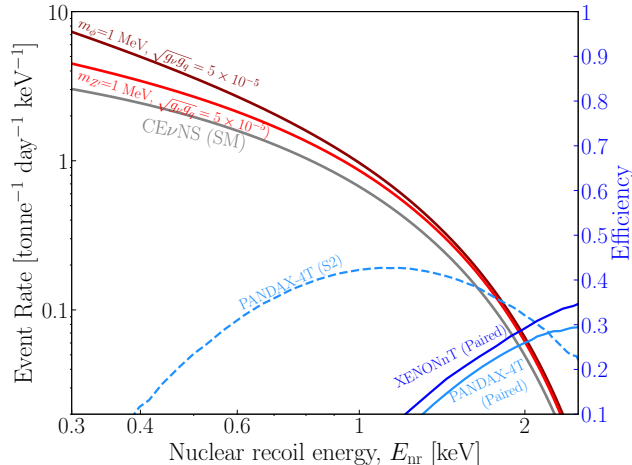
2.3. A Leptophilic Scalar

While we are primarily interested in neutrino scattering on nuclei in this paper, we will also investigate a scenario where the scattering is predominantly on electrons. In particular, let us consider a leptophilic light scalar mediator, whose Lagrangian reads

$$\mathcal{L}_{\phi,e} \supset \phi\left(g_\nu \bar{\nu}_R \nu_L + g_e \bar{e}e + \text{h.c.}\right) - \frac{1}{2}m_\phi^2\phi^2. \qquad (16)$$

The corresponding elastic neutrino–electron scattering cross section reads (for a neutrino with flavor α)

$$\frac{d\sigma_\alpha^\phi}{dE_{\text{er}}} = \frac{g_\nu^2 g_e^2 m_e^2 E_{\text{er}}}{4\pi E_\nu^2\left(2m_e E_{\text{er}} + m_\phi^2\right)^2}. \qquad (17)$$

2.4. A New Vector Mediator

We now consider a new light vector mediator Z' coupling universally to all quarks and neutrinos, thus interacting at the detector predominantly via CEνNS. The vector mediator may also induce scattering off electrons via kinetic mixing with the SM photon [55]. Constraints on such new mediators can therefore be derived also from electron scattering experiments, see *e.g.* Refs. [11, 56], leading to the conclusion that kinetic mixing needs to be very small, given current theoretical and experimental bounds [57–59]. We will therefore work with the simplified Lagrangian (neglecting kinetic mixing)

$$\mathcal{L} \supset g_q \bar{q}\gamma^\alpha Z'_\alpha q + g_\nu \bar{\nu}\gamma^\alpha Z'_\alpha \nu\,. \qquad (18)$$

Note that, unlike for the scalar mediator, the Z'-mediated CEνNS amplitude can interfere with the SM one. The total scattering cross section taking both contributions into account is obtained from Eq. (1) by replacing the vector charge according to

$$Q_V \to Q_V + \frac{3 g_q g_\nu}{\sqrt{2}G_F}\frac{(Z+N)\,F_N(E_{\text{nr}})}{2m_A E_{\text{nr}} + m_{Z'}^2}\,. \qquad (19)$$

Again the differential event rate then follows from Eq. (10). In the following, we assume positive couplings $g_q g_\nu$, which leads to constructive interference in the scattering cross section.

3. PANDAX-4T AND XENONNT CONSTRAINTS ON LIGHT MEDIATORS

3.1. Main Results

We are now ready to calculate the expected neutrino scattering event rates in PANDAX-4T and XENONnT, and to set limits on possible new physics contributions to the observed CEνNS rate. We begin in Fig. 2 by showing the differential scattering rate for the SM and for extensions featuring a scalar or vector mediator, both with flavor-universal couplings to quarks. In both BSM sce-

FIG. 2. Scattering rates for CEνNS in the SM (gray), compared to scenarios with a new flavor-universal light scalar (dark red) or vector (light red) mediator. In both cases, we have assumed flavor-universal couplings. We also show the total efficiencies of the PandaX-4T and XENONnT analyses from Refs. [1, 2] (blue curves / right vertical axis). The plot clearly reveals the enhancement $\propto 1/E_{\rm nr}$ of the scalar-induced scattering processes compared to the SM at low energies, as expected from Eq. (14).

| | PandaX-4T | | XENONnT |
	S1+S2	S2 only	S1+S2
exposure [tonne yrs]	1.20	1.04	3.51
observed events $N_{\rm obs}$	1	158	37
background events $N_{\rm bck}$	2.16	144	38.3
signal events scalar benchmark	1.04	30.52	6.55
signal events vector benchmark	1.11	44.32	8.05

TABLE I. Experimental parameters used in our analysis, based on Ref. [1] for PandaX-4T and on Ref. [2] for XENONnT. The last two rows show numbers of expected signal events for two benchmark scenarios, corresponding, respectively, to a new flavor-universal scalar or vector with for $m_{\phi,Z'} = 1\,{\rm MeV}$, $g_\phi = 5.2 \times 10^{-6}$, $g_{Z'} = 1.5 \times 10^{-5}$.

CEνNS rate due to new physics:

$$N_{\rm sig}^{\rm PA,S1+S2} < 2.01 \qquad \text{(PANDAX-4T, S1+S2)} \qquad (20)$$

$$N_{\rm sig}^{\rm PA,S2} < 35.5 \qquad \text{(PANDAX-4T, S2 only)} \qquad (21)$$

$$N_{\rm sig}^{\rm XE,S1+S2} < 9.71 \qquad \text{(XENONnT, S1+S2)} \qquad (22)$$

By imposing that the event rate for a given parameter point shall not exceed these limits, we find the upper limits on the new mediator mass m_ϕ or $m_{Z'}$, and on the product of couplings $g_\nu g_q$ shown in Fig. 3. The four panels of this figure correspond to a scalar mediator with universal couplings to quarks according to Eq. (12) (top left), a scalar mediator with quark mass-dependent couplings (top right), a vector mediator according to Eq. (18) (bottom left), and a leptophilic scalar (bottom right). We have verified our procedure by checking that our upper limit on a new heavy vector mediator is comparable to the limit on new four-fermion interactions derived in Ref. [15]. For this comparison, we relate the couplings g_ν, g_q to the dimensionless parameters ϵ_q from Ref. [15] via $\epsilon_q = g_\nu g_q/(2\sqrt{2}G_F m_{Z'}^2)$.

The qualitative shape of the PANDAX-4T and XENONnT bounds is the same in all panels of Fig. 3: they scale as m_ϕ^{-1} down to mediator masses $m_\phi \simeq 2m_A E_{\rm er} \sim 30\,{\rm MeV}$ (or $m_\phi \simeq 2m_e E_{\rm er} \sim 10\,{\rm keV}$ in the case of neutrino–electron scattering for the leptophilic mediator). At lower mediator masses, the curves flatten out, as can be easily understood from Eqs. (1), (14) and (19). The PANDAX-4T S2-only limits present a slightly different m_ϕ dependence compared to XENONnT and PANDAX-4T S1+S2 because the PANDAX-4T S2-only analysis is sensitive down to lower recoil energies (see in Fig. 2). Overall, PANDAX-4T's S2-only data nevertheless provides the least stringent of the limits derived here due to the smaller exposure.

Comparing the top left and bottom left panels of Fig. 3, we note that the limits on vector mediators are less tight than those for flavor-universal scalar mediators by a factor of ~ 2. This may at first seem surprising, given that new vector interactions interfere constructively with the SM contributions, while for new scalar interactions, there

narios, we observe an increased scattering rate compared to the SM at low energies. This can be easily understood from Eqs. (14) and (19): as long as m_ϕ is negligible compared to the typical momentum transfer in the scattering process, the differential cross section scales as $1/E_{\rm nr}$. Considering the detection efficiencies shown in blue in Fig. 2, we see that liquid xenon detectors are beginning to be sensitive to recoil energies low enough to benefit from this enhancement. Nevertheless, detection of nuclear recoil energies below $1\,{\rm keV}$ remains challenging. We note the appreciable difference between the efficiency curve for the S2-only analysis in PANDAX-4T compared to XENONnT: PANDAX-4T is sensitive down to lower recoil energies, while XENONnT's maximum efficiency is higher, though only at nuclear recoil energies above $1\,{\rm keV}$.

Based on the differential scattering rates and efficiencies, together with the exposure times, background predictions, and observed number of events summarized in Table I, we can constrain the coupling of new light mediators. We compute the ratio of the Poisson likelihoods of the observed event number in both a background-only scenario and in the scenario including new physics. By Wilks' theorem [66], this likelihood ratio follows a χ^2 distribution if the number of events is sufficiently large, so we can set limits based on the quantiles of the χ^2 probability distribution. We find the following upper limits at 90% confidence level on the extra contribution to the
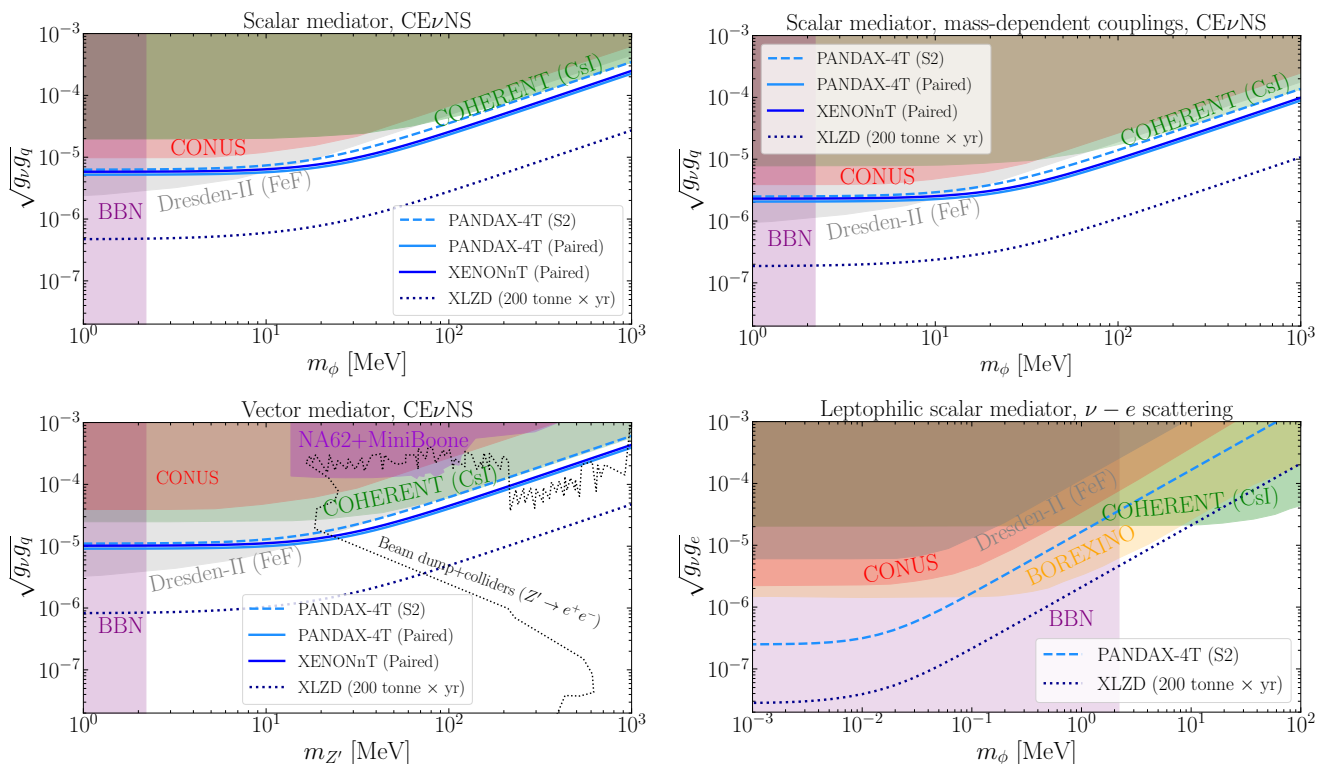
FIG. 3. **Top left:** limits on the mass and couplings of a new scalar mediator (see Eq. (12)), from the requirement that coherent elastic neutrino–nucleus scattering (CEνNS) mediated by this new particle shall not violate the 90% C.L. constraints from PANDAX-4T (light blue) and XENONnT (blue). We show results for both the S1+S2 analysis (solid) and for the S2-only analysis, but find no significant differences in sensitivity. We also show the expected sensitivity of a hypothetical detector with an exposure of 200 tonne yrs (dark blue dotted). The green region is ruled out by measurements of CEνNS in the cesium iodide (CsI) detectors of COHERENT. We further show upper limits from the CONUS [60] and Dresden-II [44] experiments. The parameter region shaded in purple is excluded by Big Bang Nucleosynthesis (BBN) [61]. **Top right:** analogous imits on the mass and couplings of a new scalar mediator with couplings to quarks proportional to the quark masses, see Eq. (13). **Bottom left:** constraints on CEνNS mediated by a light vector with interactions given by Eq. (18). Compared to scalar mediators, we further show bounds in shaded orange on a leptophobic vector from NA62 [62] and MiniBoone [63]. Furthermore, the region to the left of the dotted black line is excluded by a combination of collider and beam dump experiments when the Z' can decay into electron-positron pairs [64]. These constraints are significantly relaxed for vector mediators which do not couple to electrons at tree-level.**Bottom right:** constraints on neutrino–electron scattering through a new leptophilic scalar mediator (see Eq. (16)) from the PANDAX-4T S2-only analysis. We compare to limits from BBN, Borexino, CONUS, COHERENT (CsI), and Dresden-II [65].

is no interference. However, the scalar charge of the nucleus is larger than the vector charge, which overcompensates for the absence of interference.

We have also derived projected upper limits for the planned XENON–LUX–ZEPLIN–DARWIN (XLZD) experiment [67], which is expected to achieve an exposure of 200 tonne yrs. We assume an energy threshold of $E_{\rm thr}^{\rm XLZD} = 0.1\,{\rm keV}$, an efficiency equal to 1 in the ROI, and an upper limit on the number of signal events of $N_{\rm sig}^{90\%,{\rm XLZD}} < 2.71$. As expected, we find a significant enhancement of the sensitivity by about one order of magnitude with respect to to current limits. Such an enhancement can become important to probe neutrinophilic dark matter models at the MeV scale [68].

3.2. Comparison with Other Limits

Let us now compare the limits we have derived from PANDAX-4T and XENONnT data to those from other CEνNS experiments, notably COHERENT [17, 69], CONUS [60] and Dresden-II [44, 70]. Further details on how we obtain the COHERENT limits are given in the Appendix. For CONUS, we use a low-energy quenching factor derived from a Lindhard model with parameter $k = 0.16$. For Dresden-II, we use a quenching factor determined using iron-filtered monochromatic neutrons (Fef) [44]; see Ref. [71] for an analysis of Dresden-II data using the Lindhard model instead). The plots show that the dependence of the CEνNS limits from PANDAX-4T and XENONnT on the mediator mass is different from the one in COHERENT [69]. Direct detection ex-

periments have a lower recoil energy threshold $E_{R,\text{thr}}$ than COHERENT, so according to the scaling arguments given above the new physics-mediated scattering cross section scales linearly with the mediator mass down to lower m_ϕ, $m_{Z'}$. Consequently, while at mediator masses m_ϕ, $m_{Z'} \gtrsim 50\,\text{MeV}$, our bounds are comparable to those from COHERENT, they are stronger by a factor of ~ 2–4 at lower masses. Compared to Dresden-II, PANDAX-4T and XENONnT CEνNS bounds are weaker at m_ϕ, $m_{Z'} \lesssim 1\,\text{MeV}$, but stronger at larger mediator masses. (If Dresden-II data is analyzed using a quenching factor based on the Lindhard model, the crossing points shifts from $\sim 1\,\text{MeV}$ to $\sim 3\,\text{MeV}$.)

At masses below $m_\phi \lesssim 1\,\text{MeV}$, new light mediators are also strongly constrained by the Big Bang Nucleosynthesis (BBN) bound on new relativistic particle species [72].[5]. Finally, for the vector mediator, strong complementary constraints exist from collider and beam-dump experiments [24], which already exclude a significant portion of parameter space accessible to CEνNS (see upper gray region in Fig. 3 right). However, these bounds are based on decays of the new mediator to electrons. Therefore, they only apply if the corresponding coupling exists. In other words, for a leptophobic vector which couples to neutrinos and quarks, but not significantly to charged leptons, these bounds would not apply. Such a scenario can be realized, for instance, if neutrinos mix with sterile states charged under gauged baryon number [3, 4].

3.3. Limits on Leptophilic Scalar Mediators

We finally discuss the constraints on leptophilic scalar mediators shown in the bottom right panel of Fig. 3. In deriving these limits, we have included the ^{8}B, CNO, ^{7}Be and pp solar neutrino fluxes, where the latter is by far the dominant contribution to neutrino–electron scattering in the ROI of PANDAX-4T and XENONnT. We find that solar neutrinos from ^{8}B, CNO and ^{7}Be contribute less than 1% to the total electron scattering rate in the ROI of PANDAX-4T. We focus here on the PANDAX-4T S2-only analysis, since in the combined S1+S2 data sets, electron recoil events are efficiently subtracted. To convert the efficiency curves shown in Fig. 2 from nuclear recoil to electron recoil equivalent energies, we use the Lindhard model with $k = 0.133 Z^{2/3} A^{-1/2}$ [74]. Furthermore, neglecting BSM physics arising from CEνNS, we can use an upper limit on the number of signal events of $N_{\text{sig}}^{\text{XE,S1+S2}} < 9.71$. We have also derived projected limits from the future XLZD experiment, using the same experimental parameters as above.

We find that the limits from PANDAX-4T (S2) improve upon those obtained from complementary labora-

tory experiments like BOREXINO, CONUS, Dresden-II and COHERENT at sufficiently small mediator masses $m_\phi \lesssim 0.1\,\text{MeV}$ thanks to the smaller energy threshold compared to BOREXINO and the larger exposure compared to CONUS. However, the existence of such light scalars would be in tension with BBN. PANDAX-4T is not competitive with BOREXINO and COHERENT at larger mediator masses, and only a future XLZD-type detector could achieve a (marginal) improvement.

4. CONCLUSIONS

The recent observation of a "fog" or "floor" of solar neutrino interactions in the dark matter direct detection experiments PANDAX-4T and XENONnT marks a milestone in astroparticle physics, opeing a new window to possible physics beyond the SM in the neutrino sector. In the first part of the present paper, we have discussed the event rates due to CEνNS, the Migdal effect, and neutrino–electron scattering in the energy window of interest to dark matter experiments. The fact that the Migdal effect and neutrino–electron scattering are non-negligible impacts in particular the analyses based solely on the ionization signal (S2-only anlyses). (In nuclear recoil analyses, the Migdal effect is included in the quenching factor calibration, and neutrino–electron scattering events are efficiently rejected.)

We have then derived novel constraints on light scalar and vector mediators using both the S1+S2 and the S2-only datasets of PANDAX-4T and XENONnT. We have found that both experiments provide leading constraints at mediator masses $\lesssim 50\,\text{MeV}$ thanks to their extremely low energy thresholds and low background rates. At larger mediator masses, their constraints are similar to those from COHERENT.

Large-scale dark matter direct detection experiments have become exquisite neutrino detectors, and a precise understanding of the event rate at these experiments is not only crucial to claim a future potential dark matter signal, but also to elucidate if neutrinos have interactions beyond the Standard Model.

---

[5] Weaker but complementary constraints to the ones derived in Ref. [72] could be obtained with the observation of a future Supernovae [73].

NOTE ADDED

During the completion of this work, Ref. [75] appeared discussing the impact of light mediators on elastic neutrino–electron scattering and CEνNS at PANDAX-4T and XENONnT. Our results are qualitatively comparable to these, but we also derive prospects for the future XLZD experiment. We further discuss the impact of the Migdal effect in these experiments.

A. DERIVING LIMITS FROM THE CSI DETECTORS IN COHERENT

COHERENT is an experiment designed to measure coherent elastic neutrino–nucleus scattering (CEνNS) using neutrinos from a stopped-pion source. In 2017, the experiment achieved the first observation of CEνNS [17], and it has since released a substantial amount of additional data [76]. Here, we explain our procedure for fitting this data.

COHERENT present their data as a list of events, each characterized by its reconstructed energy, $E_{\rm rec}$, and time relative to the arrival of the primary proton beam spill, $t_{\rm rec}$. The expected number of events in the i-th energy bin and j-th time bin is

$$N^{ij} = N_T \int dt\, dE_{\rm rec}\, dE_{\rm nr}\, dE_\nu\, \varepsilon_E(E_{\rm rec})\, \varepsilon_t(t_{\rm rec})$$

$$\times\, \mathcal{R}(E_{\rm rec}, E_{\rm nr}) \sum_{\substack{\alpha=\mu,\bar{\mu},e \\ A={\rm Cs,I}}} \frac{d\sigma^{\alpha A}(E_{\rm nr}, E_\nu)}{dE_{\rm nr}} f^\alpha(E_\nu)\, g^\alpha(t_{\rm rec}),$$

(A1)

where E_ν is the neutrino energy, $E_{\rm nr}$ is the nuclear recoil energy, $\frac{d\sigma^{\alpha A}}{dE_{\rm nr}}$ is the CEνNS cross-section for neutrinos of flavor α on target nuclei of species A (see Eq. (1)),
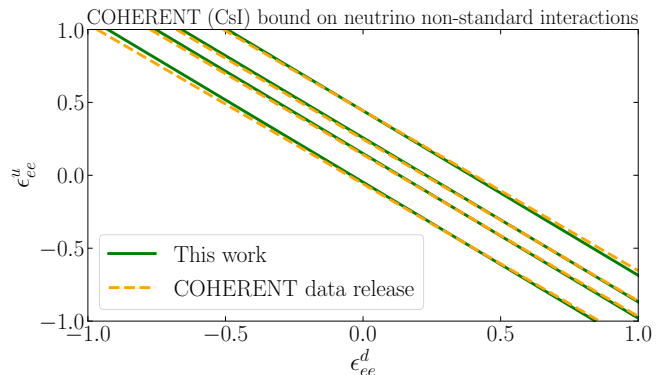

FIG. 4. 90% C.L. bounds on neutrino non-standard interactions (via the parameters ϵ_{ee}^u and ϵ_{ee}^d) from CEνNS at COHERENT (CsI). Our bounds (green) are compared to those from Ref. [76] (orange).

and the detector response function $\mathcal{R}(E_{\rm rec}, E_{\rm nr})$ maps nuclear recoil energies onto reconstructed energies. The functions $\varepsilon_E(E_{\rm rec})$ and $\varepsilon_t(t_{\rm rec})$ are efficiency factors. Finally, $f(E_\nu)\, g(t_{\rm rec})$ is the neutrino flux, factorized into an energy spectrum and a time profile. The function $f(E_\nu)$ is taken from Ref. [77], while the others inputs are taken from the COHERENT data release accompanying Ref. [76] as ancillary files. The sum in the second line of Eq. (A1) runs over the three neutrino flavors produced in π^+ decay and over the two target isotopes. The integrals over $t_{\rm rec}$ and $E_{\rm rec}$ run over the width of bin (ij), while the $E_{\rm nr}$ integral runs over the interval $(0, m_\mu/2)$, where m_μ is the muon mass. For the neutrino energy, the integration is performed over the range $(E_\nu^{\rm min}, E_\nu^{\rm max})$, where $E_\nu^{\rm min}$ is the minimum neutrino energy for a given recoil energy (see Eq. (4)) and $E_\nu^{\rm max}$ corresponds to the endpoint for each flavor in π^+ decay.

We consider three sources of background: a steady-state background, and two beam related backgrounds, namely beam-related neutrons and neutrino-induced backgrounds. These are described and parametrized in the supplementary materials of the data release accompanying Ref. [76].

To incorporate the effect of a new light mediator we add to the cross section in Eq. (A1) the new physics contribution according to Eqs. (14) and (17) for the scalar mediator, or according to Eq. (1) with the replacement Eq. (19), which yields comparable results to [54].

Finally we perform a maximum-likelihood fit using a Poissonian χ^2 to comparing the predicted event rate to the observed one from Ref. [76]. We introduce six nuisance parameters that parameterize variations in the neutrino-to proton-yield (essentially, the normalization for the number of events), the normalization of the three backgrounds, the energy efficiency parameters (assumed to be fully correlated), and the time at which the neutrino burst sets on. The latter nuisance parameter is left unconstrained, while the rest are assumed to be small.

This yields the bounds shown in Fig. 3, which are

comparable (up to a factor ~ 1.5) to those obtained in Ref. [69] for CsI in both the scalar and vector cases. We further compare our results with those from the COHERENT data release in Ref. [76] in Fig. 4. In this plot, we show in particular bounds on neutrino–quark non-standard interaction parameters (corresponding to the limit where the mediator mass squared is much larger than the momentum transfer of the scattering). It can be appreciated that our bounds agree very well with those from the experimental data release.

[1] Zihao Bo *et al.* (PandaX), "First Measurement of Solar ^{8}B Neutrino Flux through Coherent Elastic Neutrino-Nucleus Scattering in PandaX-4T," (2024), arXiv:2407.10892 [hep-ex].

[2] E. Aprile *et al.* (XENON), "First Measurement of Solar ^{8}B Neutrinos via Coherent Elastic Neutrino-Nucleus Scattering with XENONnT," (2024), arXiv:2408.02877 [nucl-ex].

[3] Maxim Pospelov, "Neutrino Physics with Dark Matter Experiments and the Signature of New Baryonic Neutral Currents," Phys. Rev. D **84**, 085008 (2011), arXiv:1103.3261 [hep-ph].

[4] Roni Harnik, Joachim Kopp, and Pedro A. N. Machado, "Exploring nu Signals in Dark Matter Detectors," JCAP **07**, 026 (2012), arXiv:1202.6073 [hep-ph].

[5] David G. Cerdeño, Malcolm Fairbairn, Thomas Jubb, Pedro A. N. Machado, Aaron C. Vincent, and Céline Bœhm, "Physics from solar neutrinos in dark matter direct detection experiments," JHEP **05**, 118 (2016), [Erratum: JHEP 09, 048 (2016)], arXiv:1604.01025 [hep-ph].

[6] Bhaskar Dutta, Shu Liao, Louis E. Strigari, and Joel W. Walker, "Non-standard interactions of solar neutrinos in dark matter experiments," Phys. Lett. B **773**, 242–246 (2017), arXiv:1705.00661 [hep-ph].

[7] D. Aristizabal Sierra, Bhaskar Dutta, Shu Liao, and Louis E. Strigari, "Coherent elastic neutrino-nucleus scattering in multi-ton scale dark matter experiments: Classification of vector and scalar interactions new physics signals," JHEP **12**, 124 (2019), arXiv:1910.12437 [hep-ph].

[8] Ian M. Shoemaker, Yu-Dai Tsai, and Jason Wyenberg, "Active-to-sterile neutrino dipole portal and the XENON1T excess," Phys. Rev. D **104**, 115026 (2021), arXiv:2007.05513 [hep-ph].

[9] Gonzalo Herrera, "A neutrino floor for the Migdal effect," JHEP **05**, 288 (2024), arXiv:2311.17719 [hep-ph].

[10] Dorian W. P. Amaral, David Cerdeno, Andrew Cheek, and Patrick Foldenauer, "A direct detection view of the neutrino NSI landscape," JHEP **07**, 071 (2023), arXiv:2302.12846 [hep-ph].

[11] Valentina De Romeri, Dimitrios K. Papoulias, and Christoph A. Ternes, "Light vector mediators at direct detection experiments," JHEP **05**, 165 (2024), arXiv:2402.05506 [hep-ph].

[12] Shuo-yu Xia, "Measuring Solar neutrino Fluxes in Direct Detection Experiments in the Presence of Light Mediators," (2024), arXiv:2410.01167 [hep-ph].

[13] Anirban Majumdar, Dimitrios K. Papoulias, Hemant Prajapati, and Rahul Srivastava, "Constraining low scale Dark Hypercharge symmetry at spallation, reactor and Dark Matter direct detection experiments," (2024), arXiv:2411.04197 [hep-ph].

[14] Gang Li, Chuan-Qiang Song, Feng-Jie Tang, and Jiang-Hao Yu, "Constraints on neutrino non-standard interactions from COHERENT and PandaX-4T," (2024), arXiv:2409.04703 [hep-ph].

[15] D. Aristizabal Sierra, N. Mishra, and L. Strigari, "Implications of first neutrino-induced nuclear recoil measurements in direct detection experiments," (2024), arXiv:2409.02003 [hep-ph].

[16] Tarak Nath Maity and Celine Boehm, "Weak mixing angle at direct detection," (2024), arXiv:2409.04385 [hep-ph].

[17] D. Akimov *et al.* (COHERENT), "Observation of Coherent Elastic Neutrino-Nucleus Scattering," Science **357**, 1123–1126 (2017), arXiv:1708.01294 [nucl-ex].

[18] Peter B. Denton, Yasaman Farzan, and Ian M. Shoemaker, "Testing large non-standard neutrino interactions with arbitrary mediator mass after COHERENT data," JHEP **07**, 037 (2018), arXiv:1804.03660 [hep-ph].

[19] D. Aristizabal Sierra, Valentina De Romeri, and N. Rojas, "COHERENT analysis of neutrino generalized interactions," Phys. Rev. D **98**, 075018 (2018), arXiv:1806.07424 [hep-ph].

[20] Mohammad Abdullah, James B. Dent, Bhaskar Dutta, Gordon L. Kane, Shu Liao, and Louis E. Strigari, "Coherent elastic neutrino nucleus scattering as a probe of a Z' through kinetic and mass mixing effects," Phys. Rev. D **98**, 015005 (2018), arXiv:1803.01224 [hep-ph].

[21] Amir N. Khan and Werner Rodejohann, "New physics from COHERENT data with an improved quenching factor," Phys. Rev. D **100**, 113003 (2019), arXiv:1907.12444 [hep-ph].

[22] O. G. Miranda, D. K. Papoulias, G. Sanchez Garcia, O. Sanders, M. Tórtola, and J. W. F. Valle, "Implications of the first detection of coherent elastic neutrino-nucleus scattering (CEvNS) with Liquid Argon," JHEP **05**, 130 (2020), [Erratum: JHEP 01, 067 (2021)], arXiv:2003.12050 [hep-ph].

[23] Heerak Banerjee, Bhaskar Dutta, and Sourov Roy, "Probing Lμ-Lτ models with CEνNS: A new look at the combined COHERENT CsI and Ar data," Phys. Rev. D **104**, 015015 (2021), arXiv:2103.10196 [hep-ph].

[24] M. Atzori Corona, M. Cadeddu, N. Cargioli, F. Dordei, C. Giunti, Y. F. Li, E. Picciau, C. A. Ternes, and Y. Y. Zhang, "Probing light mediators and $(g-2)_\mu$ through detection of coherent elastic neutrino nucleus scattering at COHERENT," JHEP **05**, 109 (2022), arXiv:2202.11002 [hep-ph].

[25] J. Billard, L. Strigari, and E. Figueroa-Feliciano, "Implication of neutrino backgrounds on the reach of next generation dark matter direct detection experiments," Phys. Rev. D **89**, 023524 (2014), arXiv:1307.5458 [hep-ph].

[26] Ciaran A. J. O'Hare, "New Definition of the Neutrino Floor for Direct Dark Matter Searches," Phys. Rev. Lett. **127**, 251802 (2021), arXiv:2109.03116 [hep-ph].

[27] Nicole F. Bell, James B. Dent, Jayden L. Newstead, Subir Sabharwal, and Thomas J. Weiler, "Migdal effect and

photon bremsstrahlung in effective field theories of dark matter direct detection and coherent elastic neutrino-nucleus scattering," Phys. Rev. D **101**, 015012 (2020), arXiv:1905.00046 [hep-ph].

[28] Rouven Essig, Mukul Sholapurkar, and Tien-Tien Yu, "Solar Neutrinos as a Signal and Background in Direct-Detection Experiments Searching for Sub-GeV Dark Matter With Electron Recoils," Phys. Rev. D **97**, 095029 (2018), arXiv:1801.10159 [hep-ph].

[29] Jason Wyenberg and Ian M. Shoemaker, "Mapping the neutrino floor for direct detection experiments based on dark matter-electron scattering," Phys. Rev. D **97**, 115026 (2018), arXiv:1803.08146 [hep-ph].

[30] Ben Carew, Ashlee R. Caddell, Tarak Nath Maity, and Ciaran A. J. O'Hare, "Neutrino fog for dark matter-electron scattering experiments," Phys. Rev. D **109**, 083016 (2024), arXiv:2312.04303 [hep-ph].

[31] Daniel Z. Freedman, "Coherent Neutrino Nucleus Scattering as a Probe of the Weak Neutral Current," Phys. Rev. D **9**, 1389–1392 (1974).

[32] J. Engel, "Nuclear form factors for the scattering of weakly interacting massive particles," Physics Letters B **264**, 114–119 (1991).

[33] J. N. Bahcall, William A. Fowler, Jr. Iben, I., and R. L. Sears, "Solar Neutrino Flux." Astrophys. J. **137**, 344–346 (1963).

[34] Núria Vinyoles, Aldo M. Serenelli, Francesco L. Villante, Sarbani Basu, Johannes Bergström, M. C. Gonzalez-Garcia, Michele Maltoni, Carlos Peña Garay, and Ningqiang Song, "A new Generation of Standard Solar Models," Astrophys. J. **835**, 202 (2017), arXiv:1611.09867 [astro-ph.SR].

[35] Edoardo Vitagliano, Irene Tamborra, and Georg Raffelt, "Grand Unified Neutrino Spectrum at Earth: Sources and Spectral Components," Rev. Mod. Phys. **92**, 45006 (2020), arXiv:1910.11878 [astro-ph.HE].

[36] M. Agostini et al. (Borexino), "Improved measurement of ^{8}B solar neutrinos with 1.5kty of Borexino exposure," Phys. Rev. D **101**, 062001 (2020), arXiv:1709.00756 [hep-ex].

[37] A. Migdal, "Ionizatsiya atomov pri yadernykh reaktsiyakh," Sov. Phys. JETP **9**, 1163 (1939).

[38] Masahiro Ibe, Wakutaka Nakano, Yutaro Shoji, and Kazumine Suzuki, "Migdal Effect in Dark Matter Direct Detection Experiments," JHEP **03**, 194 (2018), arXiv:1707.07258 [hep-ph].

[39] G. Plante, E. Aprile, R. Budnik, B. Choi, K. L. Giboni, L. W. Goetzke, R. F. Lang, K. E. Lim, and A. J. Melgarejo Fernandez, "New Measurement of the Scintillation Efficiency of Low-Energy Nuclear Recoils in Liquid Xenon," Phys. Rev. C **84**, 045805 (2011), arXiv:1104.2587 [nucl-ex].

[40] Wei Mu, Xiaonu Xiong, and Xiangdong Ji, "Scintillation Efficiency for Low-Energy Nuclear Recoils in Liquid-Xenon Dark Matter Detectors," Astropart. Phys. **61**, 56–61 (2015), [Erratum: Astropart.Phys. 72, 109–109 (2016)], arXiv:1306.0170 [physics.ins-det].

[41] M Szydagis, N Barry, K Kazkaz, J Mock, D Stolp, M Sweany, M Tripathi, S Uvarov, N Walsh, and M Woods, "Nest: a comprehensive model for scintillation yield in liquid xenon," Journal of Instrumentation **6**, P10002–P10002 (2011).

[42] E. Aprile et al. (XENON100), "Response of the XENON100 Dark Matter Detector to Nuclear Recoils,"

[43] Phys. Rev. D **88**, 012006 (2013), arXiv:1304.1427 [astro-ph.IM].

Chung-Chun Hsieh, Lakhwinder Singh, Chih-Pan Wu, Jiunn-Wei Chen, Hsin-Chang Chi, C. P Liu, Mukesh K. Pandey, and Henry T. Wong, "Discovery potential of multiton xenon detectors in neutrino electromagnetic properties," Phys. Rev. D **100**, 073001 (2019), arXiv:1903.06085 [hep-ph].

[44] Pilar Coloma, Ivan Esteban, M. C. Gonzalez-Garcia, Leire Larizgoitia, Francesc Monrabal, and Sergio Palomares-Ruiz, "Bounds on new physics with data of the Dresden-II reactor experiment and COHERENT," JHEP **05**, 037 (2022), arXiv:2202.10829 [hep-ph].

[45] Gonzalo Herrera and Patrick Huber, "Anapole moment of neutrinos and radioactive sources near liquid xenon detectors," (2024), arXiv:2408.11904 [hep-ph].

[46] Jiunn-Wei Chen, Hsin-Chang Chi, C. P. Liu, and Chih-Pan Wu, "Low-energy electronic recoil in xenon detectors by solar neutrinos," Phys. Lett. B **774**, 656–661 (2017), arXiv:1610.04177 [hep-ex].

[47] P. Vogel and J. Engel, "Neutrino Electromagnetic Form-Factors," Phys. Rev. D **39**, 3378 (1989).

[48] Jingke Xu et al., "Search for the Migdal effect in liquid xenon with keV-level nuclear recoils," Phys. Rev. D **109**, L051101 (2024), arXiv:2307.12952 [hep-ex].

[49] Jeanne Bang, "Migdal search in lux-zeplin dark matter experiment," in Talk at the UCLA Dark Matter 2023 Conference (Los Angeles, CA, 2023).

[50] J Lindhard, V Nielsen, M Scharff, and P V Thomsen, "Integral equations governing radiation effects. (notes on atomic collisions, iii)," Kgl. Danske Videnskab., Selskab. Mat. Fys. Medd. **33** (1963).

[51] Yasaman Farzan, Manfred Lindner, Werner Rodejohann, and Xun-Jie Xu, "Probing neutrino coupling to a light scalar with coherent neutrino scattering," JHEP **05**, 066 (2018), arXiv:1802.05171 [hep-ph].

[52] Enrico Bertuzzo, Frank F. Deppisch, Suchita Kulkarni, Yuber F. Perez Gonzalez, and Renata Zukanovich Funchal, "Dark Matter and Exotic Neutrino Interactions in Direct Detection Searches," JHEP **04**, 073 (2017), arXiv:1701.07443 [hep-ph].

[53] Martin Hoferichter, J. Ruiz de Elvira, Bastian Kubis, and Ulf-G. Meißner, "High-Precision Determination of the Pion-Nucleon σ Term from Roy-Steiner Equations," Phys. Rev. Lett. **115**, 092301 (2015), arXiv:1506.04142 [hep-ph].

[54] Martin Hoferichter, Javier Menéndez, and Achim Schwenk, "Coherent elastic neutrino-nucleus scattering: Eft analysis and nuclear responses," Physical Review D **102** (2020), 10.1103/physrevd.102.074018.

[55] Bob Holdom, "Two U(1)'s and Epsilon Charge Shifts," Phys. Lett. B **166**, 196–198 (1986).

[56] Amir N. Khan, "Constraints on general light mediators from PandaX-II electron recoil data," Phys. Lett. B **819**, 136415 (2021), arXiv:2008.10279 [hep-ph].

[57] Andrea Caputo, Alexander J. Millar, Ciaran A. J. O'Hare, and Edoardo Vitagliano, "Dark photon limits: A handbook," Phys. Rev. D **104**, 095029 (2021), arXiv:2105.04565 [hep-ph].

[58] Arthur Hebecker, Joerg Jaeckel, and Ruben Kuespert, "Small kinetic mixing in string theory," JHEP **04**, 116 (2024), arXiv:2311.10817 [hep-th].

[59] James M. Cline and Gonzalo Herrera, "Plausible constraints and inflationary production for dark photons,"

(2024), arXiv:2409.13818 [hep-ph].

[60] H. Bonet *et al.* (CONUS), "Novel constraints on neutrino physics beyond the standard model from the CONUS experiment," JHEP **05**, 085 (2022), arXiv:2110.02174 [hep-ph].

[61] Guo-yuan Huang, Tommy Ohlsson, and Shun Zhou, "Observational Constraints on Secret Neutrino Interactions from Big Bang Nucleosynthesis," Phys. Rev. D **97**, 075009 (2018), arXiv:1712.04792 [hep-ph].

[62] Eduardo Cortina Gil *et al.* (NA62), "Search for production of an invisible dark photon in π^0 decays," JHEP **05**, 182 (2019), arXiv:1903.08767 [hep-ex].

[63] A. A. Aguilar-Arevalo *et al.* (MiniBooNE), "Dark Matter Search in a Proton Beam Dump with MiniBooNE," Phys. Rev. Lett. **118**, 221803 (2017), arXiv:1702.02688 [hep-ex].

[64] Matt Graham, Christopher Hearty, and Mike Williams, "Searches for Dark Photons at Accelerators," Ann. Rev. Nucl. Part. Sci. **71**, 37–58 (2021), arXiv:2104.10280 [hep-ph].

[65] Pilar Coloma, , M. C. Gonzalez-Garcia, Michele Maltoni, João Paulo Pinheiro, and Salvador Urrea, "Constraining new physics with Borexino Phase-II spectral data," JHEP **07**, 138 (2022), [Erratum: JHEP 11, 138 (2022)], arXiv:2204.03011 [hep-ph].

[66] S. S. Wilks, "The Large-Sample Distribution of the Likelihood Ratio for Testing Composite Hypotheses," Annals Math. Statist. **9**, 60–62 (1938).

[67] J. Aalbers *et al.*, "A next-generation liquid xenon observatory for dark matter and neutrino physics," J. Phys. G **50**, 013001 (2023), arXiv:2203.02309 [physics.ins-det].

[68] Jeffrey M. Berryman *et al.*, "Neutrino self-interactions: A white paper," Phys. Dark Univ. **42**, 101267 (2023), arXiv:2203.01955 [hep-ph].

[69] V. De Romeri, O. G. Miranda, D. K. Papoulias, G. Sanchez Garcia, M. Tórtola, and J. W. F. Valle, "Physics implications of a combined analysis of CO-HERENT CsI and LAr data," JHEP **04**, 035 (2023), arXiv:2211.11905 [hep-ph].

[70] J. Colaresi, J. I. Collar, T. W. Hossbach, C. M. Lewis, and K. M. Yocum, "Measurement of Coherent Elastic Neutrino-Nucleus Scattering from Reactor Antineutrinos," Phys. Rev. Lett. **129**, 211802 (2022), arXiv:2202.09672 [hep-ex].

[71] D. Aristizabal Sierra, V. De Romeri, and D. K. Papoulias, "Consequences of the Dresden-II reactor data for the weak mixing angle and new physics," JHEP **09**, 076 (2022), arXiv:2203.02414 [hep-ph].

[72] Nikita Blinov, Kevin James Kelly, Gordan Z Krnjaic, and Samuel D McDermott, "Constraining the Self-Interacting Neutrino Interpretation of the Hubble Tension," Phys. Rev. Lett. **123**, 191102 (2019), arXiv:1905.02727 [astro-ph.CO].

[73] Anna M. Suliga and Irene Tamborra, "Astrophysical constraints on nonstandard coherent neutrino-nucleus scattering," Phys. Rev. D **103**, 083002 (2021), arXiv:2010.14545 [hep-ph].

[74] Thomas Schwemberger and Tien-Tien Yu, "Detecting beyond the standard model interactions of solar neutrinos in low-threshold dark matter detectors," Phys. Rev. D **106**, 015002 (2022), arXiv:2202.01254 [hep-ph].

[75] Valentina De Romeri, Dimitrios K. Papoulias, and Christoph A. Ternes, "Bounds on new neutrino interactions from the first CEνNS data at direct detection experiments," (2024), arXiv:2411.11749 [hep-ph].

[76] D. Akimov *et al.* (COHERENT), "Measurement of the Coherent Elastic Neutrino-Nucleus Scattering Cross Section on CsI by COHERENT," Phys. Rev. Lett. **129**, 081801 (2022), arXiv:2110.07730 [hep-ex].

[77] Pilar Coloma, Ivan Esteban, M.C. Gonzalez-Garcia, and Michele Maltoni, "Improved global fit to non-standard neutrino interactions using coherent energy and timing data," Journal of High Energy Physics **2020** (2020), 10.1007/jhep02(2020)023.